

EXPERIMENTAL STUDY OF EXTENDED TARGET IMAGING BY TIME REVERSAL SAR

Yuanwei Jin

Engineering and Aviation Sciences
University of Maryland Eastern Shore
Princess Anne, MD 21853
yjjin@umes.edu

José M.F. Moura and Nicholas O'Donoghue *

Electrical and Computer Engineering
Carnegie Mellon University
Pittsburgh, PA 15213
{moura, nodonoug}@ece.cmu.edu

ABSTRACT

Conventional SAR images under rich scattering suffer degradation because of ghost images caused by multipath propagation. In this paper, we develop a time reversal SAR (TR-SAR) imaging algorithm for extended (nonpoint-like) targets in rich multipath scattering. We test the TR-SAR algorithm using experimental electromagnetic data collected in a laboratory environment where the extended target (a galvanized steel sheet) is surrounded by a large amount of PVC rods. Our experiments show that the collected EM data in frequency and aperture after TR-SAR processing produces a higher resolution, cleaner target map compared with conventional SAR images.

Index Terms— Time Reversal, Extended Target Imaging, Synthetic Aperture Radar (SAR)

1. INTRODUCTION

Synthetic aperture radar (SAR) systems provide a crucial reconnaissance technology for many commercial and military applications. Typical SAR systems are designed for imaging targets with a direct line of sight of the SAR sensors. However, in a environment where the intended target (for example, man-made objects such as a tank or a truck) is hidden or surrounded by many scatterers (for example, trees with large tree trunks), the target signature consists of the directly returned waveform as well as the secondary reflected waveforms due to surrounding scatterers. SAR images of the intended target under such a scattering environment manifest themselves as the true target image (due to the direct return) and the ghost images (due to the secondary returns). The ghost images severely degrade the resolution of SAR images as well as the subsequent automatic target recognition (ATR) performance.

In [1, 2], we developed a time reversal based SAR algorithm for imaging a point target and removing ghost images that are caused by multipath scattering. In our previous work, we demonstrate that time reversal is a powerful technique to achieve improved imaging resolution and detection [3, 4]. In this paper, we study the problem of imaging extended (nonpoint-like) targets using time reversal combined with spotlight mode synthetic aperture radar. We verified the imaging results using electromagnetic data collected in a laboratory with a rich scattering environment. The extended target has a simple shape, but allows varying orientation and

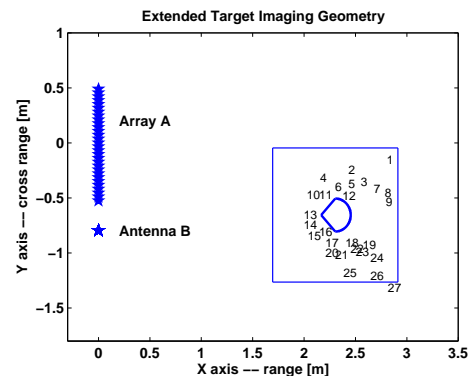


Fig. 1. Geometry of bistatic spotlight SAR in squint mode for an extended target (a half circle and triangle joined by welding: array A with aperture $u \in [-L, L]$ is centered at the origin, and antenna B is at a fixed location (X_B, Y_B)). The ground patch is centered at (X_c, Y_c) . The numbers indicate the scatterer locations.

placement in the field of view of the antenna. Related work is that of [5, 6, 7], where the time-reversal MUSIC method is applied to the location of extended targets. We should also note that we do not consider the multiple-bounce scattering from an extended target [8]. Our focus is on the multipath scattering due to the surrounding scatterers of an extended target.

In this paper, we analyze and test the developed time-reversal SAR algorithm for extended targets that are surrounded by many scatterers in a laboratory environment. The objective is to remove ghost images and create a clean target map for imaging the extended target.

2. SIGNAL MODEL

We assume that the background environment is stationary and can be overviewed before the target appears. First, we probe the environment using pulse $P(\omega)$ and obtain the clutter response $S_c(\omega, u)$ at the receive antenna, where u denotes the position of the antenna in the cross range of the imaging scene. The symbol ω denotes the angular frequency. We then enter the monitoring phase where we continuously probe the environment. The goal is now to decide if a target comes into the environment. The received response is $S_{c+t}(\omega, u)$ that con-

*This work is funded by the Defence Advanced Research Projects Agency through the Army Research Office under grant no. W911NF-04-1-0031.

sists of the target response plus the clutter response. Due to our assumption that the background environment is stationary, we obtain the target signature by subtracting $S_c(\omega, u)$ from $S_{c+t}(\omega, u)$ as

$$S(\omega, u) = S_{c+t}(\omega, u) - S_c(\omega, u). \quad (1)$$

We also assume that an extended target consists of a cluster of point reflectors; each reflector is characterized by its radar cross section and the phase term that is due to its relative position with respect to the SAR sensor. The number of scattering centers of an extended target that a radar can identify is limited by the radar resolution. The extended target under test appears to show two dominant scattering centers given the operation frequency range and the synthetic aperture size of our experiment. Hence, for simplicity, we use a two-point target model as follows:

$$S(\omega, u) = P(\omega) \left[\tau_1 e^{-jkR_1(u)} H_1(\omega, u) + \tau_2 e^{-jkR_2(u)} H_2(\omega, u) \right], \quad (2)$$

where $k = \frac{\omega}{c}$ is the wave number and $\tau_i, i = 1, 2$, is the i -th radar cross section (RCS) of the point-like reflector of the extended target. For each point-like reflector located at $(X_c + x_i, Y_c + y_i)$, $i = 1, 2$, we let

$$R_i(u) = \sqrt{(X_c + x_i)^2 + (Y_c + y_i - u)^2} + \sqrt{(X_c + x_i - X_B)^2 + (Y_c + y_i - Y_B)^2}$$

denote the distance between the aperture at $(0, u)$, the point reflector, and antenna B at (X_B, Y_B) (see Fig. 1 for illustration). The quantity

$$H_i(\omega, u) = 1 + \sum_{l=1}^L \alpha_{i,l} e^{-jk\Delta R_{i,l}(u)} \quad (3)$$

denotes the normalized multipath target response for the i -th point reflector. The quantity $\alpha_{i,l}$ and

$$\Delta R_{i,l}(u) = R_{i,l}(u) - R_i(u), \quad l = 1, \dots, L \quad (4)$$

are the relative amplitude and distance of the l -th multipath, respectively. Furthermore, we assume that

$$H_1(\omega, u) \approx H_2(\omega, u). \quad (5)$$

This assumption is valid because (1) for an extended target in a far field relative to the SAR sensor, the scattering conditions for each reflector are very similar; (2) in rich scattering, the aggregate effect of a large amount of scatterers makes a few strong scatterers close to the extended target negligible. Hence, we can re-write (2) as

$$S(\omega, u) = P(\omega) \left[\tau_1 e^{-jkR_1(u)} + \tau_2 e^{-jkR_2(u)} \right] H_1(\omega, u). \quad (6)$$

3. TR-SAR

TR-SAR processing aims to improve the resolution of conventional SAR images under rich scattering environment. TR-SAR is implemented by the following steps: (1) **Multilook**

averaging of conventional SAR images. In this step, the full aperture SAR phase history data is divided into several looks (subaperture). Each subaperture is processed to produce subaperture images. These images are registered and averaged to produce a single image. Because ghost patterns due to surrounding scatterers to a target are look-angle dependent [1], multilook averaging essentially removes the ghost patterns and retains the true target image. However, the penalty paid is loss of resolution. (2) **Radar cross section estimation from averaged SAR intensity image.** In this step, we estimate the radar cross section of the point-like reflector based on the SAR intensity image. Related work is that of [9] where the RCS of point targets is estimated when the speckle noise is removed. Here we let

$$\hat{\tau}_i = a\tau_i, \quad i = 1, 2 \quad (7)$$

denote the estimate of the RCS of the i -th point reflector, where a is the unknown scaling factor. In our experiment, the speckle noise is negligible. The RCS of the scattering center can be obtained by estimating the reflectivity directly from the SAR intensity image. For simplicity, here we assume that the intensity scaling is the same for the point reflectors that belong to the same extended target. Furthermore, let (\hat{x}_i, \hat{y}_i) be the rough estimate of the i -th point reflector location, which yields

$$\hat{R}_i(u) = \sqrt{(X_c + \hat{x}_i)^2 + (Y_c + \hat{y}_i - u)^2} + \sqrt{(X_c + \hat{x}_i - X_B)^2 + (Y_c + \hat{y}_i - Y_B)^2}.$$

(3) Construct time-reversal signals for re-transmission.

We first construct the target response filter

$$\hat{T}(\omega, u) = \hat{\tau}_1 e^{jk\hat{R}_1(u)} + \hat{\tau}_2 e^{jk\hat{R}_2(u)} \quad (8)$$

The estimated target response filter $\hat{T}(\omega, u)$ is multiplied by $S(\omega, u)$, which yields

$$P_{\text{tr}}(\omega, u) = k_u [\hat{T}(\omega, u) S(\omega, u)]^* \quad (9)$$

where the energy normalization factor is given by

$$k_u = \sqrt{\frac{\int |P(\omega)|^2 d\omega}{\int |\hat{T}(\omega, u) S(\omega, u)|^2 d\omega}}. \quad (10)$$

We note that the unknown scalar a in (7) will be canceled through the normalization.

(4) **TR-SAR image reconstruction.** The energy normalized, time reversed signal is transmitted. Assume that the channel is reciprocal, the received signal becomes

$$S_{\text{tr}}(\omega, u) = P_{\text{tr}}(\omega, u) \left[\tau_1 e^{-jkR_1(u)} + \tau_2 e^{-jkR_2(u)} \right] \times H_1(\omega, u) \quad (11)$$

$$= k_u [\hat{T}(\omega, u) S(\omega, u)]^* \left[\tau_1 e^{-jkR_1(u)} + \tau_2 e^{-jkR_2(u)} \right] \times H_1(\omega, u) \quad (12)$$

$$= k_u P^*(\omega) |H_1(\omega, u)|^2 \left[\hat{\tau}_1 e^{-jk\hat{R}_1(u)} + \hat{\tau}_2 e^{-jk\hat{R}_2(u)} \right] \left\{ \tau_1^2 + \tau_2^2 + 2\tau_1\tau_2 \cos[k(R_1(u) - R_2(u))] \right\} \quad (13)$$

For simplicity, if the estimate of the target location and RCS is accurate, i.e., $\hat{R}_i(u) = R_i(u)$, we obtain

$$S_{\text{tr}}(\omega, u) = (ak_u)P^*(\omega)|H_1(\omega, u)|^2 \left[\tau_1 e^{-jkR_1(u)} + \tau_2 e^{-jkR_2(u)} \right] \{ \tau_1^2 + \tau_2^2 + 2\tau_1\tau_2 \cos[k(R_1(u) - R_2(u))] \}. \quad (14)$$

If we compare (6) with (14), we see that the number of phase terms in (14) is reduced to two, i.e., $e^{-jkR_1(u)}$ and $e^{-jkR_2(u)}$, which represents the two point reflectors of the extended target. This implies that the ghost images due to multipath scattering are removed. Furthermore, the term

$$|H_1(\omega, u)|^2 = \left| 1 + \sum_{l=1}^L \alpha_{i,l} e^{-jk\Delta R_{i,l}(u)} \right|^2 \quad (15)$$

resembles a sinc-like function proportional to the number of path of L (see [2]). Implementing the matched filter based SAR algorithm [10], we use

$$S_0(\omega, u) = P^*(\omega) e^{-jkR_0(u)}. \quad (16)$$

as the reference signal that shifts the focusing point of the image to the center of the ground patch (X_c, Y_c) and implements data compression for subsequent FFT processing. Thus, a final image is then produced by taking the inverse Fourier Transform of [10]:

$$S_{\text{tr}}(\omega, u) S_0^*(\omega, u), \quad (17)$$

which yields

$$f(x, y) = \int_{\omega} \int_{k_u} d\omega dk_u e^{jk_x(\omega, k_u)x + jk_y(\omega, k_u)y} J(\omega, k_u) |P(\omega)|^2 \sum_{i=1}^2 |\tau_i|^2 \mathcal{F}(u) \left[(\tau_1^2 + \tau_2^2 + 2\tau_1\tau_2 \cos[k(R_1(u) - R_2(u))]) (ak_u) |H_1(\omega, u)|^2 e^{-jk(R_i(u) - R_0(u))} \right], \quad (18)$$

where $J(\omega, k_u)$ is the Jacobian of the transformation from $[k_x(\omega, k_u), k_y(\omega, k_u)]$ to (ω, k_u) .

4. EXPERIMENTAL RESULTS

Fig. 1 depicts the experimental setup for imaging an extended target. The extended target, shown as a joint semi-circle and triangle, is placed 2.3 meters away from the antenna arrays and is surrounded by a total of 27 PVC rods and other scatterers. The relative locations of the scatterers are indicated by numbers. The target is a 6 feet tall, galvanized steel sheet. It is constructed by welding a triangle and a semi-circle. The diameter of the semi-circle is 30 cm, the edge length of the triangle is 21 cm. The target itself has a very smooth surface, hence, it is anticipated that the scattered EM waves emanating from the target are caused mainly by reflection. To enhance multipath scattering, the target is wrapped with crinkled foil

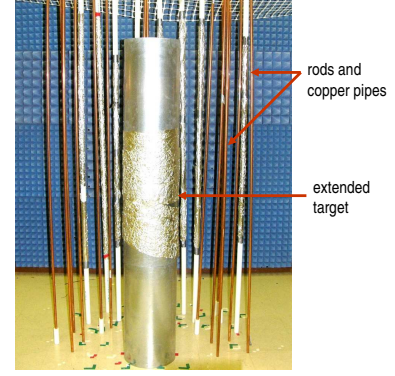


Fig. 2. Photo of experimental setup for time reversal extended target imaging.

to increase surface roughness. Fig. 2 shows the extended target standing on the floor, surrounded by many scatterers. Note that the PVC rods are wrapped with aluminum foil to enhance signal reflection. An absorber wall is placed behind the scatterers to avoid reflections from outside the scattering environment.

The two-dimension SAR data is measured by a network analyzer working in the range of 4 – 6 GHz. We collect a total of 201 sample points in the frequency domain. These frequency sample points are the range data. The cross range data is obtained by moving the antenna along a position slider. The position slider is 1 meter long. We collect frequency samples at a total of 30 positions along the position slider. Hence, we obtain the data samples $S_c(\omega_q, u_n)$, where $n = 1, \dots, 30$, and $q = 0, \dots, 200$. We measure the scattering scene twice: the first time, we measure the clutter only environment, the reflected radar data is organized as $S_c(\omega_q, u_n)$; then, we place the extended target among the scatterers, the reflected radar data is organized as $S_{c+t}(\omega_q, u_n)$. The discrete target response data, denoted by

$$S(\omega_q, u_n) = S_{c+t}(\omega_q, u_n) - S_c(\omega_q, u_n), \quad (19)$$

is used to implement the TR-SAR algorithm. We follow the procedure described in section 3 for TR-SAR processing. Due to space limitation, the multi-look processing is not presented here and will be discussed in details in another paper.

Fig. 3 depicts the conventional SAR image and the TR-SAR image of the extended target. The conventional SAR image shows two blurred pixels of the upper edge of the triangle of the target. There are also many ghost pixels that are caused by multipath scattering. Due to the orientation of the target, i.e., the upper edge of the triangle is facing the transmit antenna array A, only two dominant pixels appear. The two dominant pixels can be estimated by conventional SAR using multi-look averaging. Next, TR-SAR focuses on two pixels of the upper edge of the triangle and shows a cleaner, higher resolution image. To visually demonstrate the resolution, we project the two images along range and cross range, respectively. The projection plots are shown in Fig. 4. The range projection plot in Fig. 4 shows that TR-SAR and SAR have the same range resolution. This is because both algorithms use the same frequency bandwidth, i.e., 2 GHz. However, the TR-SAR shows two dominant main beams that correspond to

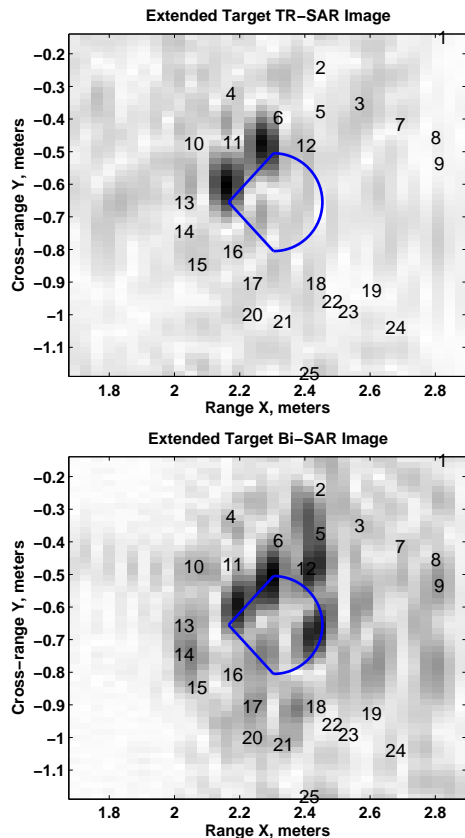


Fig. 3. Image of extended target produced by TR-SAR (upper figure) and by conventional SAR (lower figure) in the spotlight, bi-static mode. The upper edge of the triangle surface of the target is imaged. The numbers indicate the locations of scatterers.

two pixels in Fig. 3. The cross range project plot in Fig. 4 shows that the TR-SAR has improved resolution (about 15 cm) over the conventional SAR (about 30 cm) algorithm using the same aperture.

5. CONCLUSION

In this paper, we develop a time reversal SAR (TR-SAR) algorithm using a simplified two-point-reflector model for extended targets. Using experimental electromagnetic data collected in a rich scattering environment, we show that TR-SAR successfully removes ghost images that are caused by multipath scattering, and produces a cleaner target map compared with conventional SAR.

6. REFERENCES

[1] Y. Jin, J. M. F. Moura, M. Mulford, N. O'Donoghue, and A. Samuel, "Time reversal synthetic aperture radar in multipath," in *Proceedings of the 41st Asilomar Conference on Signal, Systems and Computers*. Pacific Grove, CA: IEEE, November 2007, pp. 1812–1816.

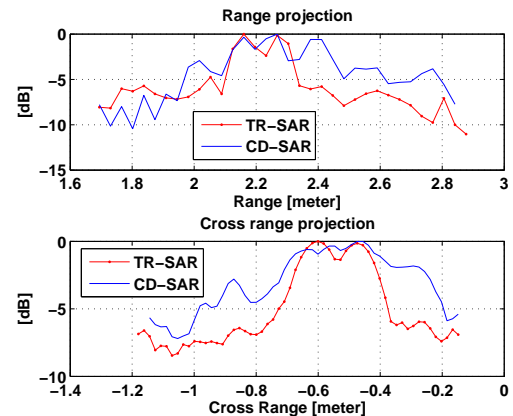


Fig. 4. Upper plot - Range resolution; Lower plot - cross range resolution. TR-SAR yields a better cross range resolution (about 15 cm) than conventional SAR (about 30 cm).

[2] Y. Jin and J. M. F. Moura, "TR-SAR: Time reversal target focusing in spotlight mode SAR," in *Proceedings of the International Conference on Acoustics, Speech, and Signal Processing*, vol. 2. Honolulu, Hawaii: IEEE, April 2007, pp. 957–960.

[3] J. M. F. Moura and Y. Jin, "Detection by time reversal: single antenna," *IEEE Transactions on Signal Processing*, vol. 51, no. 1, pp. 187–201, January 2007.

[4] —, "Imaging using time reversal: adaptive interference cancellation," *IEEE Transactions on Signal Processing*, vol. 56, no. 1, pp. 233–247, January 2008.

[5] D. H. Chambers and J. G. Berryman, "Analysis of the time-reversal operator for a small spherical scatterer in an electromagnetic field," *IEEE Transactions on Antennas and Propagation*, vol. 52, no. 7, pp. 1729–1738, July 2004.

[6] S. Hou, K. Solna, and H. Zhao, "Imaging of location and geometry for extended targets using the response matrix," *Journal of Computational Physics*, vol. 199, no. 1, pp. 317–338, September 2004.

[7] E. A. Marengo, F. K. Gruber, and F. Simonetti, "Time-reversal MUSIC imaging of extended targets," *IEEE Transactions On Image Processing*, vol. 16, no. 8, pp. 317–338, September 2007.

[8] D. A. Garren, J. S. Goldstein, and J. A. North, "Extraction of multiple-bounce echoes in SAR image formation," in *Proceedings of the Sensor Array and Multichannel Signal Processing Workshop*. IEEE, August 2002, pp. 538–542.

[9] I. McConnell, R. G. White, C. J. Oliver, and R. Cook, "Radar cross-section estimation of SAR images," in *Proceedings of the SPIE*, vol. 2584, 1995, pp. 164–175.

[10] M. Soumekh, *Synthetic Aperture Radar Signal Processing*. New York, NY: John Wiley & Sons, Inc., 1999.